Surface & Coatings Technology 285 (2016) 262–269

Contents lists available at ScienceDirect

Surface & Coatings Technology

journal homepage: www.elsevier.com/locate/surfcoat

Nanostructured CuO_x coatings onto Cu foils: Surface growth by the combination of gas-phase treatments

Claudia A. Neyertz, Agustín D. Gallo, María A. Ulla, Juan M. Zamaro *

Instituto de Investigaciones en Catálisis y Petroquímica, INCAPE (FIQ, UNL, CONICET), Santiago del Estero 2829, (3000) Santa Fe, Argentina

ARTICLE INFO

Article history:
Received 18 September 2015
Revised 10 November 2015
Accepted in revised form 1 December 2015
Available online 2 December 2015

Keywords:
Nanostructured surface
Copper oxide
Synthesis
Coating
XPS
Catalysis

ABSTRACT

In this work, the growth of copper oxide nanoarrays on the surface of copper foils by gas-based oxidation treatments was analyzed, employing either NH_3–H_2O_2 vapors or air at high temperature. By adjusting the treatment conditions, homogeneous and firmly anchored copper oxide coatings were obtained, with densely packed surface nanostructures in the form of nanowires, nanofibers or nanorods. The homogeneity and stability of these nanostructures critically depends on the surface texture of the support, which can be easily changed by sanding or $FeCl_3$ pretreatments. The sequential combination of both treatments allowed modifying the oxide nanoarchitectures and their surface composition. The NH_3–H_2O_2/air sequence led to a transformation of surface nanorods with an outermost layer of Cu_2O, first in CuO nanograins from which then CuO nanowires grew. A reverse combination, air/NH_3–H_2O_2, generated a dense growth of cobweb-like nanofibers onto a base layer of CuO nanowires. The surface oxide nanostructures obtained, distributed in a large area and firmly anchored to the support, have great potential for the development of structured catalysts.

1. Introduction

The size and shape of copper oxide crystals have a great effect on many of their properties with impact on several research fields such as magnetic storage media [1], lithium ion batteries [2], superconductors [3], sensors [4] and catalysis [5], among others. In principle, these features can be regulated by controlling the synthesis method, which has led to the appearance of an extensive literature on the synthesis of nanostructured CuO crystals with different morphologies, e.g. nanoflowers, nanosheets, nanowires, nanoleaves and nanoellipsoids, among others. Most preparation methods involve wet-based methods [6–10]. In this way, CuO nanoflowers have been synthesized on copper foils by hydrothermal treatments of the substrate with alkaline solutions containing H_2O_2 and $S_2O_8^{2-}$ [11]. Hydrothermal treatments employing different surfactants such as sodium dodecyl sulfate (SDS) [12], bromide cetyltrimethylammonium (CTAB) and surfactant Tx-1000 [13] have also been used to obtain different dimensional copper oxide nanostructures. Simpler strategies like the use of NaOH solutions have also been addressed but extremely long times are required to achieve a good density of nanostructures [14]. However, as mentioned above, the conventional wet processing methods could present difficulties for the growth of oxide nanostructures on substrates with complex geometries such as meshes, microchannels, or foams, gas-phase methods being a simpler, more convenient strategy. The synthesis of highly dispersed nano-copper oxides on these types of microstructured substrates is of great interest for the development of new reactors with enhanced catalytic performance [15]. Soejima et al. [16] reported the obtention of CuO nanobelts on the surface of copper plates using vapors of NH_3 and H_2O_2 whereas in several recent reports heat treatments in air have been used to grow CuO nanowires on various copper substrates [17–23]. In this context, the focus of the present work is to study the growth of nanostructured copper oxide films using combinations of these simple gas-based oxidation procedures. The aim of this research work is to gain insight into key preparation variables for the obtention of high quality, densely packed and well-anchored nano-oxide coatings as a platform for the future development of structured catalysts.

2. Experimental

2.1. Coating synthesis

Commercial electrolytic pure copper foils (99.9%, 100 μm thickness) in pieces of 2 × 1 cm were used. All substrates were treated with 2 N HCl during 15 min and then washed with distilled water in ultrasonic bath for 5 min. Surface modification pretreatments of some foils were carried out by sanding (sandpaper N° 1000) or by treatments with a $FeCl_3$ solution by stirring for 5 min at room temperature. One oxidation method (VAP) consisted in placing the foils suspended vertically above the liquid level in a flask (100 mL) containing 20 mL of NH_4OH (Cicarelli, pro-analysis, 37% w/w) and H_2O_2 (Cicarelli, pro-analysis, 100 vol.). The sealed reactor was heated in an oven at 80 °C and the copper surfaces were exposed to vapors. Afterwards, the foils were washed with distilled water and dried in air. The other surface oxidation treatment

* Corresponding author at: Santiago del Estero 2829, (3000) Santa Fe, Argentina.
E-mail address: zamaro@fiq.unl.edu.ar (J.M. Zamaro).

http://dx.doi.org/10.1016/j.surfcoat.2015.12.001
0257-8972/

(CAL) consisted in heating the foils in static air, for which purpose the substrates were vertically supported and heated in a muffle at different temperatures (400–750 °C) and periods (4–16 h). In addition, the calcination in air flow (30 cm^3 min^{-1}, 500 °C, 2 °C min^{-1}, 4 h) was also performed. Afterwards, a detailed analysis of the changes in the nanooxides was carried out by sequentially combining both methods, either VAP–CAL or CAL–VAP. In what follows, samples obtained via NH_3–H_2O_2 vapors are denoted as "VAP(t)m:n" where t is the treatment time and m:n are the volume ratios of NH_3 and H_2O_2, respectively. The samples obtained via calcination with air at high temperature are denoted as "CAL(t)C", where t is the treatment time and C is the temperature in °C. The names of samples prepared with combined procedures represent the order in which the methods were applied. Table S1 summarizes the prepared samples.

2.2. Sample characterization

X-ray Diffraction (XRD) was performed with a Shimadzu XD-D1 instrument by scanning the 2θ angle at 2° min^{-1} between 30° and 55° using CuKα radiation (λ = 1.5418 Å, 30 kV, 40 mA). The surface of the supports was studied with a stereomicroscope Leica S8 APO with a digital camera Leica LC3, while the microstructure of the films was examined by Scanning Electron Microscopy (SEM) with a JEOL JSM-35C operated at 20 kV. The samples were glued to the sample holder with Ag painting and then coated with a thin layer of Au in order to improve the images. X-ray Photoelectronic Spectroscopy (XPS) analyses of the coatings were carried out with a module Multitechnique Specs. The spectra were obtained with a pass energy of 30 eV with a Mg anode operated at 200 W. The pressure during the measurement was less than 2.10^{-8} mbar. The foils were supported on the sample holder, subjected to vacuum dehydration at 150 °C for 15 min and finally evacuated under vacuum prior to the readings. The peak of C 1s at 284.8 eV was taken as internal reference. The binding energies (BE) of Cu 2p, C 1s and O 1s core-levels were analyzed. The kinetic energy (KE) of the Cu LMN Auger transitions was also measured. The data processing was performed using the Casa XPS software.

3. Results and discussion

3.1. Growth of nanostructures by single methods

3.1.1. Treatment with NH_3–H_2O_2 vapors (VAP)

By applying this treatment, an increased weight gain of the foils was recorded up to 8 h reaction time but, subsequently, a reduction in the weight gain was observed, generating a volcano-type curve (Fig. 1a). This could be due to a partial redissolution of the formed oxides during a longer treatment, probably due to the fact that $Cu(OH)_4^{2+}$ complexes formed under the basic environment can be dissolved in the condensed solution on the substrate surface. The coatings formed showed the main signals of the (111) and (200) planes of the cubic Cu_2O structure (JCPDS 5-667) and also those of the monoclinic CuO structure, corresponding to the (110), (−111), (111) and (20–2) planes, respectively (JCPDS 48-1548). In addition, these foils exhibited prominent XRD peaks (Fig. 2a) corresponding to the (111) and (200) planes of Cu° of the support (JCPDS 4-836). In all cases a mixture of CuO and Cu_2O was observed, the intensity signals of the former being somewhat higher. Taking 8 h as the optimal synthesis time for an optimal weight gain, the effect of the reactant ratio was analyzed. In this case, a maximum in the weight

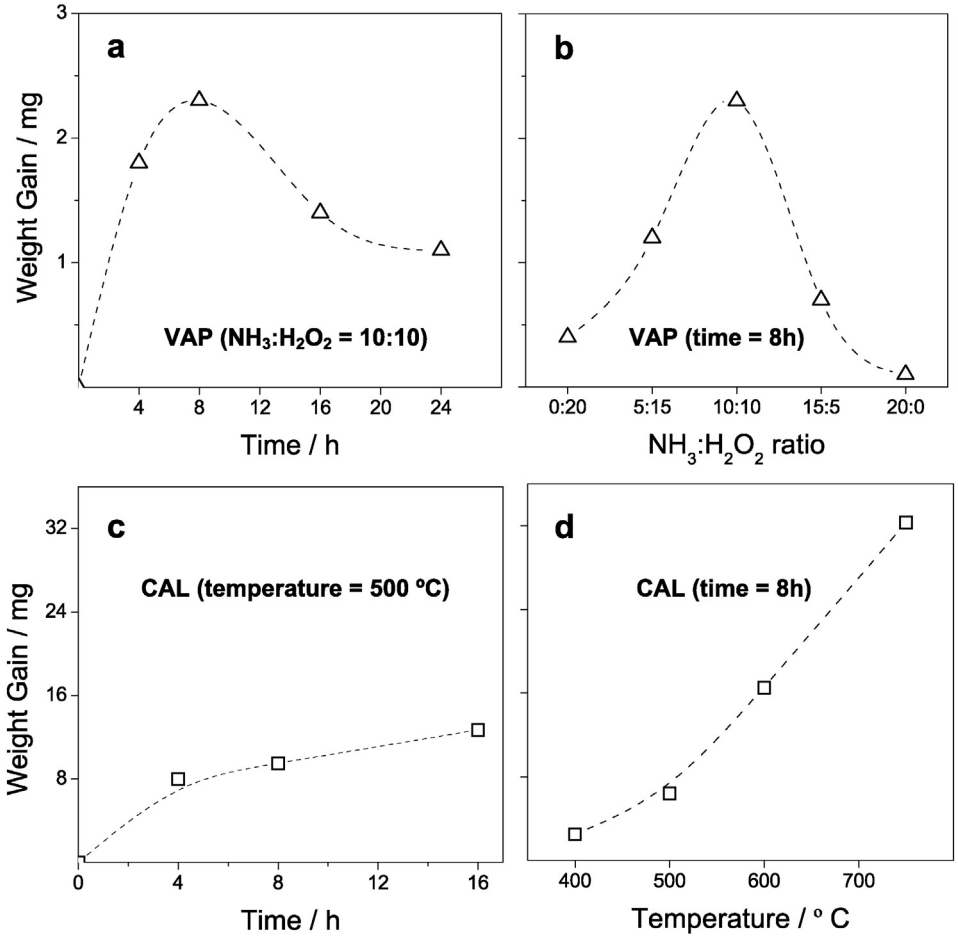

Fig. 1. Weight gain of foils: a) VAP treatment at different times; b) VAP treatment at different NH_3:H_2O_2 ratios; c) CAL treatment at different times; and d) CAL treatment at different temperatures.

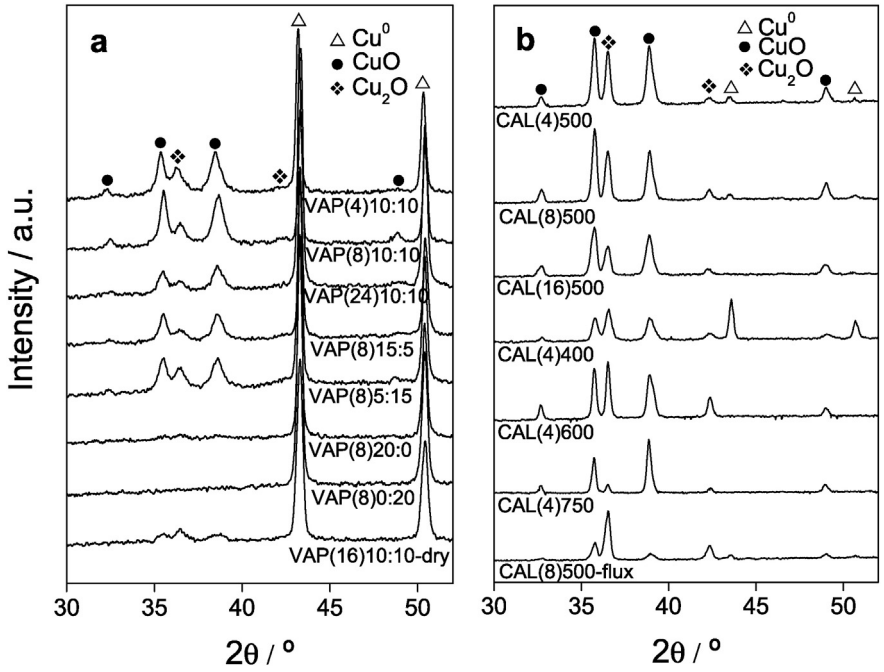

Fig. 2. XRD patterns of the foils treated by: a) VAP method; b) CAL method.

gain was also observed (Fig. 1b). It can be seen that when no NH_3 was added (VAP(8)0:20 sample) no XRD signals of oxides were detected, whereas without the addition of H_2O_2 (VAP(8)20:0 sample) very weak ones were present (Fig. 2a). This implies the need of both reagents for the surface oxidation process which is in agreement with Soejima et al.'s results [16]. According to these authors, H_2O_2 would produce the initial oxidized species on the substrate surface, which could then be complexed with NH_3. Under basic conditions, the NH_3 groups are probably replaced by OH producing $Cu(OH)_4^{2+}$ complexes that are finally transformed into CuO. However, in our samples a mixture of CuO and Cu_2O phases was present which, as discussed below, is due to the formation of a surface layer of Cu_2O. In the cases analyzed above, the surface of the wet foils were exposed to vapors immediately after the washing treatment, but when the foils were dried prior to synthesis, a reduction in both weight gain and intensity of diffraction peaks of oxides was observed (VAP(16)10:10dry sample in Fig. 2a). A thin film of water on the substrate probably allowed the dissolution of vapors and facilitated a further attack to copper.

The best microstructure of the oxide layer in this set of samples was observed in the VAP(8)10:10 sample, which showed highly packaged and well-anchored nanorods that completely covered all the support surface (Fig. 3a). The mechanical stability of this coating was high, showing no mass loss after subjecting the sample to an ultrasound treatment in water for 15 min. These nanorods grew from the upper third of the coating thickness with an average length of about 1.3 μm and a width of 180 nm (Fig. 3b). When other reactant proportions were used, low quality nanostructures were obtained. For the VAP(8)15:5 sample some isolated nanowalls-like formations were developed (Fig. S1a) while when only NH_3 was employed, a thin layer of polyhedral crystals was obtained, which copied the original topography of the support that has macro-roughness with parallel grooves (Fig. S1b). These formations would correspond to the initial growth of copper oxide grains. On the other hand, for the samples obtained during longer reaction times there appeared a film of segmented nanorods, some of them grouped in spheres deposited on the surface (Fig. S1d), which confirm a partial redissolution of the formed oxides when extending the contact time with vapors.

3.1.2. Treatment in air at high temperature (CAL)

This treatment generally produced a higher weight gain of the foils than that obtained by the VAP method and was much more affected by temperature than by time (Fig. 1c and d). This is consistent with a parabolic growth kinetics as the one proposed for the growth of oxides by thermal oxidation [20]. It is clearly seen that a treatment at 600 °C for 8 h generated a high weight gain but the simple manipulation of this sample caused the detachment of the oxide coating, while at 750 °C a degradation of the physical structure of the copper foil was produced probably due to the large amount of oxides formed. When the temperature was lower than 400 °C, a higher proportion of Cu_2O was noticed while the XRD signals of the support persisted (Fig. 2b), indicating a thinner coating thickness due to the slow formation of cuprous oxide at these temperatures [18]. It is also observed that by increasing the temperature the relative intensity of the CuO signals is enhanced while the support peaks are hardly detected.

The optimum combination of mechanical stability and weight gain of the oxide coating was achieved with treatments at 500 °C for 8 h. In this case, the mechanical stability of the coating was somewhat lower than VAP since it exhibited a mass loss of about 50% w/w after an ultrasound treatment. The surface microstructure of this sample appeared like islands of nanowires as shown in Fig. 3c, with wires about 15 μm length and 350 nm wide (Fig. 3d), whereas by reducing the treatment time to 4 h the amount of wires produced was smaller with wires shorter and narrower (2 μm and 180 nm, respectively) and the area between the islands increased (Fig. S1e). The presence of a relatively thick oxide layer in these samples (e.g. Fig. 3d and f) is consistent with the drastic reduction in the XRD signals of the copper substrate as seen in Fig. 2b. Besides, in comparison with the sample obtained at 8 h, after 16 h neither the dimensions of the nanostructures nor the islands density substantially changed (Fig. S1f). However, the mechanical stability of the coating in this latter case was lower because of the higher coating thickness. In agreement with what has been reported in recent studies [18,22], in the samples obtained by this method, we observed a layered oxide phase with a base layer from which nanowires grew. This is due because first a Cu_2O layer formed onto a copper substrate on which a thinner CuO film later developed. Then the CuO nanowires grew. The particular nanowire islands observed in our samples seem to be related

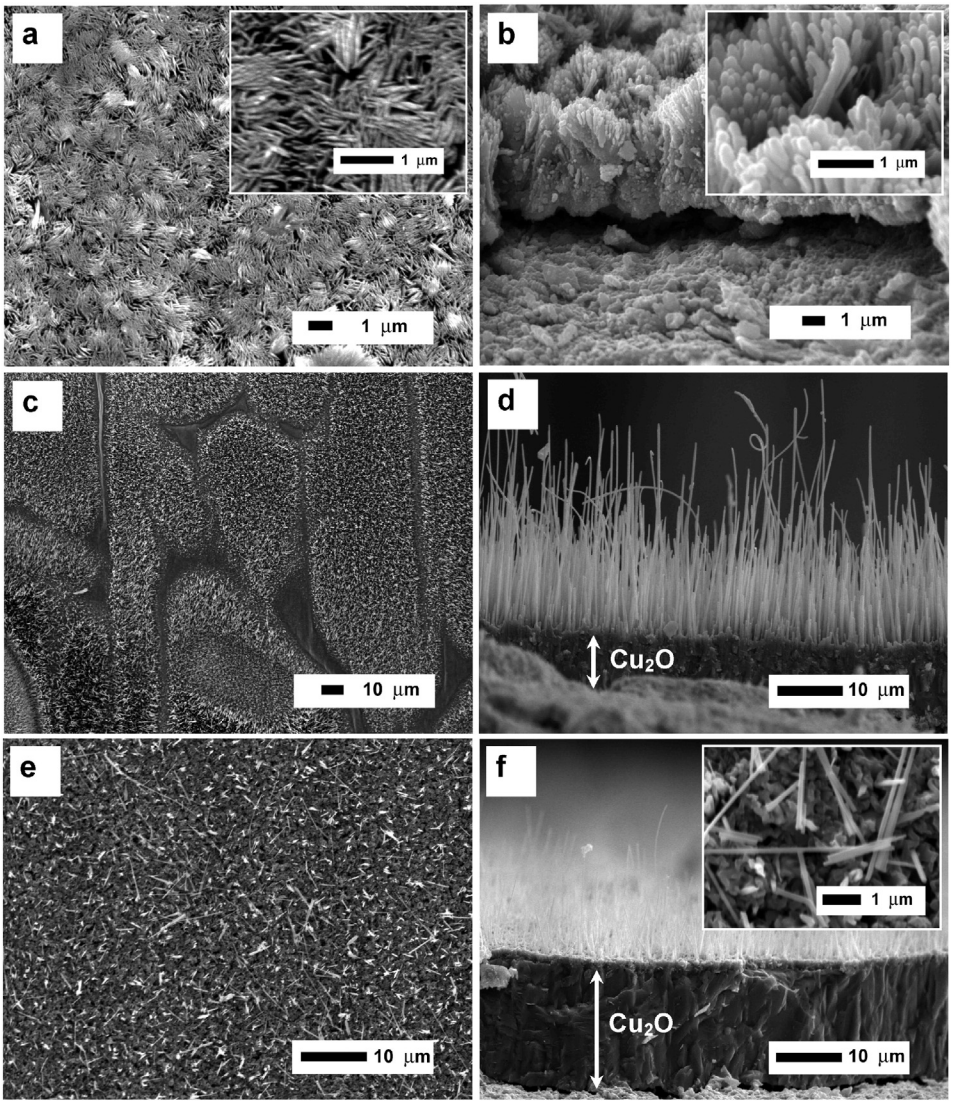

Fig. 3. SEM images of samples obtained by the CAL and VAP methods: a) VAP(8)10:10 in top view, b) VAP(8)10:10 in side view, c) CAL(8)500 in top view, d) CAL(8)500 in side view, e) CAL(8)500-flux in top view, and f) CAL(8)500-flux in side view.

to the surface defects in the bare copper foil which had micrometer size crater-like hollows (Fig. S1c). When dynamic conditions were employed, the behavior of the oxides growth notably changed. By air-flow treatments under the same conditions of time and temperature as above (CAL(8)500-flux sample), a lower mass gain (Table S1) and a higher relative proportion of Cu_2O (Fig. 2b) were obtained. This was also consistent with a low density of formed CuO nanowires (Fig. 3e) and a thicker Cu_2O base layer (Fig. 3f), compared with the static case. Probably, the higher partial pressure of oxygen at the support surface favored the first and faster step of Cu_2O formation, while the further oxidation to CuO still remained slow.

3.2. Effect of the surface texture on the nano-oxides growth

The results described above suggest a strong influence of the substrate imperfections in the nano-oxides growth. Henceforth, we studied this aspect in detail. By treating the substrate with a $FeCl_3$ solution, a smoother surface was obtained (Fig. S2) since copper is etched by the following redox reaction: $2\ FeCl_3 + Cu^0 \rightarrow 2\ FeCl_2 + CuCl_2$. On the other hand, when the substrate was sanded, the roughness increased. This is clearly seen in the optical and SEM images where a higher number of surface imperfections are evident when compared to the original substrate (Fig. S2).

By applying the VAP treatment in the substrate modified by $FeCl_3$, a more uniform surface coverage with vertically aligned nanorods was produced (Fig. 5a). This is probably due to an even distribution of nucleation sites for the nano-oxide growth on this surface. On the contrary, when the CAL treatment was applied on this support, the nanowire growth was smaller in the form of spots (Fig. 5b) and the oxide scale had a lower adhesion. The weight gain and oxide proportions in both cases were similar as those obtained on the untreated surfaces (Fig. S3). In the case of the sanded substrates, the VAP treatment produced a lesser homogeneity in the distribution of the nanorods (Fig. S4), supporting that for this method the grown nanostructures depend on the arrangement of the first copper surface species. In contrast, when the sanded substrate was subjected to CAL, a better nanostructure homogeneity was achieved with smaller boundary regions between the nanowire islands (Fig. S4), which supports the fact that the surface defects favor the formation of the wires. It should be mentioned that no difference was observed in wire dimensions (length 18 μm, width 270 nm) or in oxides proportion. For the thermal formation of nanowires, various mechanisms have been proposed, e.g. the vapor-solid mechanism [17], the short-circuit diffusion mechanism [20] and the stress-induced mechanism [21,24]. In the latter mechanism, a stress in the interface between the layer of CuO and Cu_2O produces compressive tensions and induces the growth of nanowires from the top CuO layer,

which is in line with our results. A smooth surface generated a uniform layer of Cu_2O from which the grains of CuO above it would be subjected to a lower stress, causing the formation of a smaller amount of wires. Conversely, a rougher surface would cause higher tensions in the Cu_2O layer provoking the higher magnitude of nanowire growth.

3.3. Growth of nanostructures by combined treatments

The gas-based treatments discussed above were applied sequentially under the optimized conditions, firstly treating the substrate with NH_3–H_2O_2 vapors and subsequently in static air at different temperatures. For the VAP–CAL300 sample, the weight gain in the first stage (VAP) was not modified in the second step (CAL) due to the low magnitude of the thermal oxidation at 300 °C. Furthermore, the relative proportion of cuprous oxide, which is the predominant phase at low temperatures, increased (Fig. 4). The nanorod structures were maintained, but the CAL step originated some thin curved nanowires (length 1.5 μm, width 70 nm) as shown in Fig. 5c, that began to grow from semispherical formations of grains. These are reaction products of the nanorods generated during the CAL step. It may be noted that nanowires did not develop from initial nanorods, and need the transformation of these into nanograins (Fig. 5e). When a VAP sample was treated at higher temperatures by CAL the proportion of CuO increased (VAP–CAL400 and VAP–CAL500 samples) as shown in Fig. 4. Furthermore, the transformation of nanorods in nanograins evolved, and the surface was covered by thin nanowires as shown in the VAP–CAL500 sample (Fig. 5d). It is possible to observe certain areas in which semispherical nanograins were transformed into a continuous base layer of CuO from which nanowires grew. Interestingly, it is for this reason that nanowires grew radially. It could also be noted that the growth of nanowires appears at the grain boundaries of the base layer (Fig. 5f).

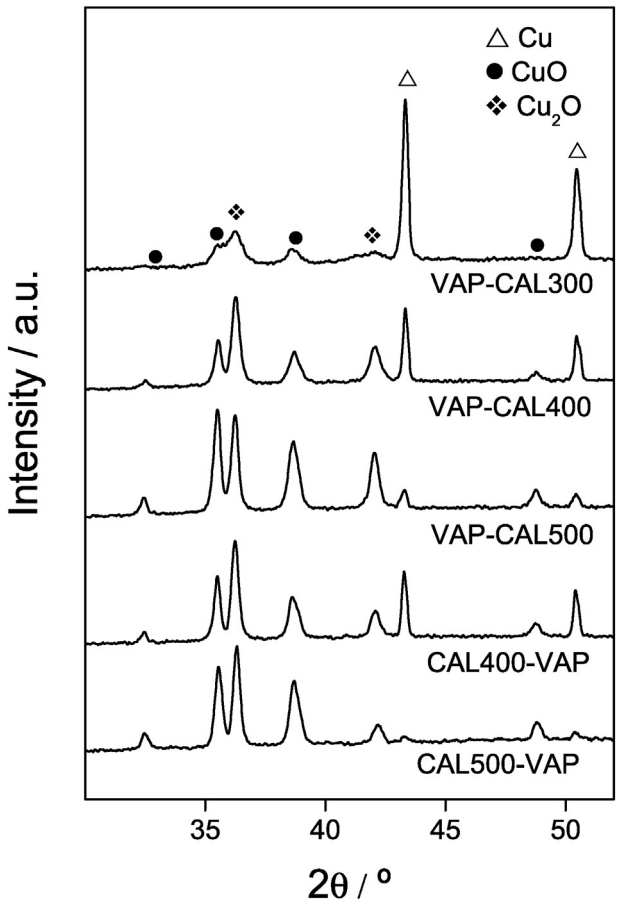

Fig. 4. XRD patterns of samples synthesized with combined gas-based methods.

By applying the inverse sequence, first a CAL treatment and then a VAP step, changes in the nanostructure composition and morphology were noticed. The CAL500–VAP sample (Fig. 4) shows a mixture of oxides similar to the CAL(8)500 sample but with a higher proportion of Cu_2O. Surprisingly, the surface of this sample was covered with a dense growth of nanofibers with a cobweb appearance, above the base layer of wires that maintained their typical vertical arrangement and dimensions (Fig. 5g). These nanofibers grew from certain wires which were entwined together and curved during the VAP treatment. Moreover, when only NH_3 was used (CAL500–VAP20:0), a growth with a nanofiber morphology similar to that of the previous case was verified (Fig. 5h). The presence of H_2O_2 in the second treatment is not necessary because a CuO phase generated in the first CAL step is already present.

3.4. Surface composition of the oxide nanostructures

The outermost layer of the nanooxide films was analyzed by XPS. The untreated copper foil (Fig. 6a) showed the characteristic Cu 2p signals of Cu° [25] with a Cu $2p_{3/2}$ peak at a Binding Energy (BE) of 932.4 eV (Table 1), while the VAP sample showed a quite similar spectrum with sharp signals at similar BEs (Table 1). The Cu 2p BEs of Cu° and Cu^+ are similar [26] and both species can be distinguished by analyzing the Auger spectrum in the Cu LMN region (Fig. 6b). The VAP sample showed the main peak at a Kinetic Energy (KE) of 916.6 eV whereas for the untreated substrate, it shifted to 919.1 eV (Table 1), which are typical values for Cu^+ and Cu° species, respectively [27]. In addition, the modified Auger parameter (α') for the VAP sample was 1849.0, which confirms the presence of superficial Cu_2O [27]. Considering the XRD results, it follows that the outermost surface layer of the nanorods is formed by cuprous oxide with a sub-layer of CuO. This can be a consequence of a NH_3 excess in the reactor chamber which can act as a reducing agent of the CuO layer, in agreement with what was reported by Wang et al. [28] and Suárez et al. [29]. The O 1s XPS region (Fig. 6d) shows a major signal around 530 eV associated with lattice oxygen and a smaller peak at higher BE (Table 1) attributed to defective oxygen in the oxide lattice and also to carbonates [26]. Unlike all the other samples, the positions of the O1s signal shifted to higher BEs since the main phase on the surface of this sample was Cu_2O and, as discussed below, in others it was CuO. These differences in the position of O1s signals coincide with those reported in the literature for such oxides [26]. The Cu/O atomic surface ratio in this sample was 1.37. On the other hand, in addition to the main C 1s signal at 284.8 eV of graphitic carbon, a contribution at higher BE was observed (Fig. 6c), which supports the presence of carbonates, probably generated by the exposure of the sample to atmospheric CO_2.

In the case of the foil treated by CAL, it shows broader Cu 2p XPS peaks with a Cu $2p_{3/2}$ signal at 933.2 eV (Table 1) and intense satellite peaks (Fig. 6a) owing to paramagnetic copper species, which confirm the presence of surface CuO. The Cu 2p signals can only be accurately fitted considering some minor Cu^+ contribution. Nevertheless, this sample shows a main Auger peak at 918.1 eV (Fig. 6b) and an α' of 1850.5 (Table 1), which are consistent with superficial CuO as primary component. The O1s and C1s regions (Fig. 6d, e) also indicate the presence of carbonates and defective oxygen that correspond to a CuO phase. The surface Cu/O ratio was 0.64 and the ratio of the Cu$2p_{3/2}$ peak area and its satellite was 3.35 (Table 1).

The VAP–CAL500 sample showed a surface transformation of Cu_2O in CuO, in line with the volumetric modifications observed by XRD and SEM, which is easily identified by the shift of the Cu XPS signals to higher BEs and to the appearance of satellite peaks (Fig. 6a). The Auger spectrum (Fig. 6b) also shows a shift of the main peak to 918.0 eV and α' was 1850.6 (Table 1). Besides, the Cu/O and Cu$2p_{3/2}$/satellite ratios show values similar to those exhibited by the CAL sample, thus confirming that the surface of the coating was completely transformed into CuO. In addition, the content of oxygen from lattice defects

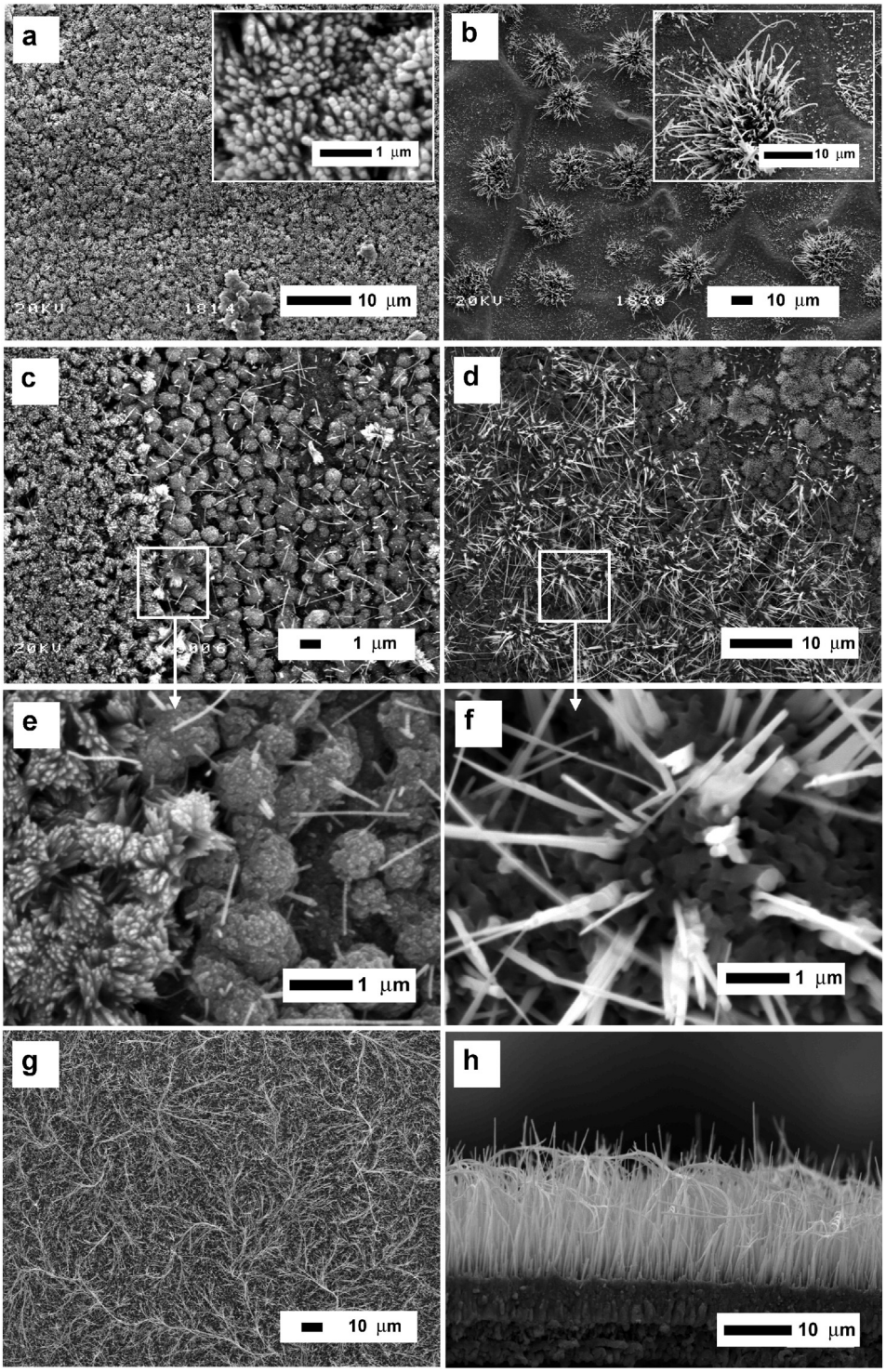

Fig. 5. SEM images of samples synthesized on pretreated substrates and with combined methods: a) VAP(8)10:10 on substrate pretreated with $FeCl_3$; b) CAL(8)500 on substrate pretreated with $FeCl_3$; c) VAP–CAL300 sample; d) VAP–CAL500 sample; e) close view of the VAP–CAL300 sample; f) close view of the VAP–CAL500 sample; g) CAL500–VAP sample; and h) CAL500–VAP sample without H_2O_2 (side view).

and carbonates increased to 45% of the total oxygen (Fig. 6d). On the other hand, when applying the CAL–VAP sequence, although the XPS spectrum showed CuO signals mainly (Fig. 6a), the $Cu2p_{3/2}$/satellite ratio was 30% higher than that of the sample obtained via the single CAL treatment. This confirms a certain proportion of surface Cu^+ produced during the VAP step as a result of a superficial CuO reduction due to an excess of NH_3, as discussed above. This means that the grown nanofibers probably have a surface layer of Cu_2O. Although the α' value (Table 1) and the Auger spectrum point out that CuO is the main compound on the surface, a broadening in the Auger spectrum profile around 917 eV (Fig. 6b) clearly shows the contribution of Cu_2O. Furthermore, the surface Cu/O ratio was somewhat higher than the CAL and VAP–CAL samples (Table 1).

4. Conclusions

Copper substrates densely covered with uniform, stable films of nanorods with an outermost surface layer of Cu_2O or islands of CuO

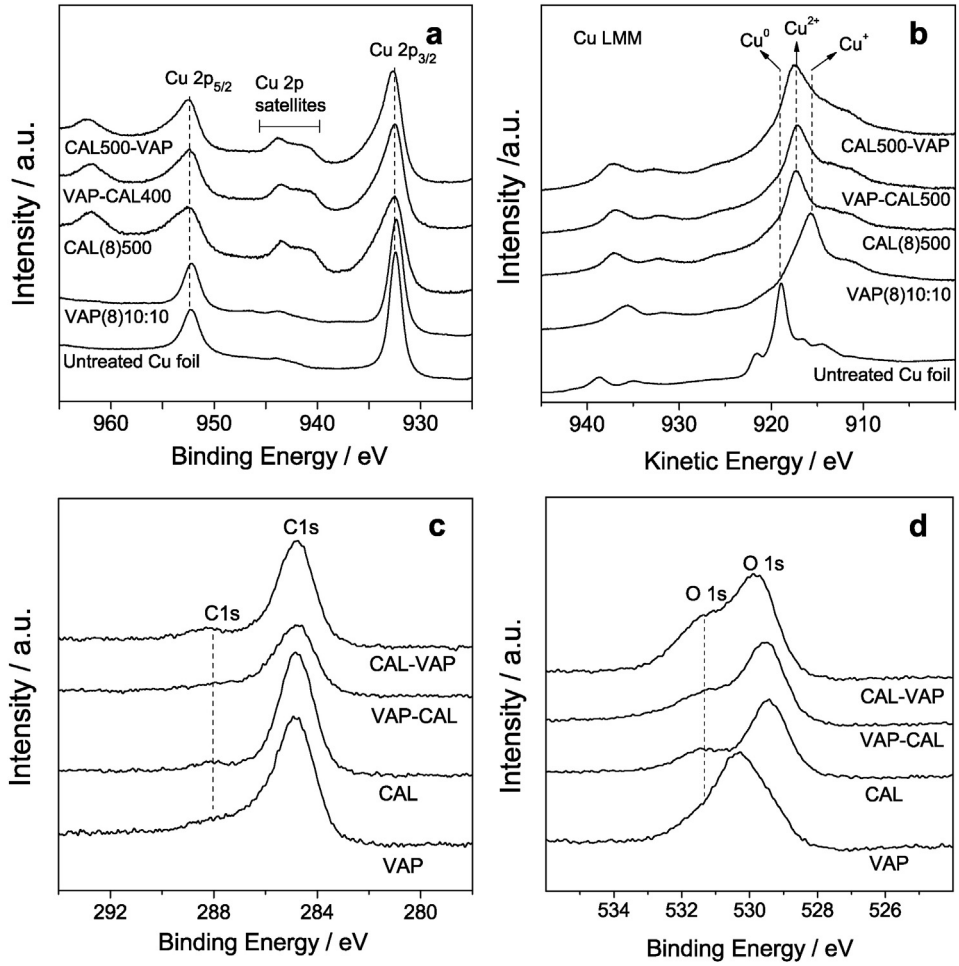

Fig. 6. XPS and Auger spectra of samples: a) XPS Cu 2p region; b) Auger Cu LMM region; c) XPS C1s region; and d) XPS O1s region.

nanowires were obtained through NH_3–H_2O_2 vapors and static air calcination treatments, respectively. From the viewpoint of nanostructure homogeneity and mechanical stability, the best results for each single method was obtained using equal proportions of H_2O_2 and NH_3 or treatments at 500 °C for 8 h (CAL), respectively. Smoother surfaces improved the nanooxide qualities with the NH_3 treatments, whereas they worsened when employing the air treatments. Conversely, a rougher surface generated a lesser homogeneity of nanorods and a greater uniformity of nanowires coverage, respectively. The combination of treatments enables to modify the oxide nanoarchitectures and their surface composition, according to the order of the successive treatment steps. The adjustment of the optimal qualities of the nanostructured coatings, namely coverage, homogeneity, adherence, and surface composition in large areas, was achieved. These nanostructures directly grown on a support with high thermal conductivity could bring about the possibility of a precise control of the coating temperature in gas-phase catalytic applications.

Table 1
Binding energies (BE), kinetic energies (KE), modified Auger parameters (α′) and elemental composition of surface nano-copper oxides.

Sample	Cu $2p_{3/2}$[a]	C 1s[a]	O 1s[a]	Cu LMM[b]	α′[c]	Cu/O	Cu $2p_{3/2}$/satellite[d]
VAP(8)10:10	932.3 (1.7)	284.8 (1.8)	530.2 (2.0)	916.6	1849.0	1.37	–
		287.1 (2.8)	532.2 (1.2)				
CAL(8)500	932.3 (1.7)	284.8 (1.6)	529.4 (1.3)	917.9	1850.5	0.64	3.35
	933.2 (3.5)	287.3 (2.8)	531.4 (1.8)				
VAP–CAL500	932.3 (1.6)	284.8 (1.8)	529.5 (1.3)	918.1	1850.6	0.64	3.61
	933.2 (3.4)	287.2 (2.8)	531.1 (2.5)				
CAL500–VAP	932.5 (1.6)	284.8 (1.7)	529.7 (1.4)	917.4	1850.8	0.78	4.38
	933.4 (3.5)	287.6 (3.4)	531.2 (2.0)				
Cu foil (untreated)	932.4 (1.6)	284.8 (1.8)	531.6 (2.5)[e]	919.1	1851.5	–	–
		286.3 (3.5)[e]					

[a] Binding energy (BE) in eV.
[b] Kinetic energy (KE) in eV.
[c] Modified Auger parameter: α′ = KE (Cu LMM) − KE (Cu $2p_{3/2}$) + 1253.6 eV.
[d] Ratio between de area of the main Cu $2p_{3/2}$ peak and its respective satellite.
[e] Signals of little intensity.

Furthermore, the nanometric interstices at the coating surface can facilitate future modifications with other metal oxide nanoparticles as catalytic promoters.

Acknowledgments

The authors thank to CONICET and the financial support received from ANPCyT (PICT 1299) and Universidad Nacional del Litoral (CAI + D 0486) for carrying out this study. Thanks are also given to ANPCyT for the purchase of the multitechnique instrument SPECS (PME8-2003), and to JICA for the XRD instrument. Thanks are finally given to Fernanda Mori and Fabio Fontanarrosa for the XPS and SEM analyses, respectively.

Appendix A. Supplementary data

Supplementary data to this article can be found online at http://dx.doi.org/10.1016/j.surfcoat.2015.12.001.

References

[1] J. Ziolo, F. Borsa, M. Corti, A. Rigamonti, F. Parmigiani, J. Appl. Phys. 67 (1990) 5864–5866.
[2] S. Bijani, M. Gabas, L. Martinez, J. Ramos-Barrado, J. Morales, L. Sanchez, Thin Solid Films 515 (2007) 5505–5511.
[3] X. Zheng, C. Xu, Y. Tomokiyo, E. Tanaka, H. Yamada, Y. Soejima, Phys. Rev. Lett. 85 (2000) 5170–5173.
[4] F. Zhang, A. Zhu, Y. Luo, Y. Tian, J. Yang, Y. Qin, J. Phys. Chem. C 114 (2010) 19214–19219.
[5] S. Bennici, A. Gervasini, Appl. Catal. B Environ. 62 (2006) 336–344.
[6] Y. Yu, J. Zhang, Mater. Lett. 63 (2009) 1840–1843.
[7] M. Vaseem, A. Umar, Y. Hahn, D. Kim, K. Lee, J. Jang, J. Lee, Catal. Commun. 10 (2008) 11–16.
[8] C. Yang, J. Wang, F. Xiao, X. Su, Powder Technol. 264 (2014) 36–42.
[9] H. Xu, W. Wang, W. Zhu, L. Zhou, M. Ruan, Cryst. Growth Des. 7 (12) (2007) 2720–2724.
[10] J. Liu, X. Huang, Y. Li, K. Sulieman, X. He, F. Sun, Cryst. Growth Des. 6 (7) (2006) 1690–1696.
[11] M. Song, S. Hwang, D. Whang, Talanta 80 (2010) 1648–1652.
[12] Q. Pan, H. Jin, H. Wang, G. Yin, Electrochim. Acta 53 (2007) 951–956.
[13] Y. Liu, Y. Chu, M. Li, L. Li, L. Dong, J. Mater. Chem. 16 (2006) 192–198.
[14] N. Ekthammathat, T. Thongtem, S. Thongtem, Appl. Surf. Sci. 277 (2013) 211–217.
[15] N. Pérez, E. Miró, J. Zamaro, Appl. Catal. B Environ. 129 (2013) 416–425.
[16] T. Soejima, H. Yagyu, N. Kimizuka, S. Ito, RCS Adv. 1 (2011) 187–190.
[17] X. Jiang, T. Herricks, Y. Xia, Nano Lett. 2 (12) (2002) 1334–1338.
[18] J. Liang, N. Kishi, T. Soga, T. Jimbo, Appl. Surf. Sci. 257 (2010) 62–66.
[19] Y. Yue, M. Chen, Y. Ju, S. Wang, J. Mater. Sci. Technol. 29 (12) (2013) 1156–1160.
[20] C. Xu, C. Woo, S. Shi, Chem. Phys. Lett. 399 (2004) 62–66.
[21] Y. Wang, R. Shen, X. Jin, P. Zhu, Y. Ye, Y. Hu, Appl. Surf. Sci. 258 (2011) 201–2016.
[22] F. Shao, F. Hernández, J. Prades, C. Fábrega, T. Andreu, J. Morante, Appl. Surf. Sci. 311 (2014) 177–181.
[23] E. Filippo, M. Tepore, T. Siciliano, D. Chirizzi, C. Malitesta, R. Guascito, Phys. E. 60 (2014) 59–64.
[24] L. Yuan, Y. Wang, R. Mema, G. Zhou, Acta Mater. 59 (2011) 2491–2500.
[25] NIST X-ray photoelectron spectroscopy database, http://srdata.nist.gov/xps.
[26] M. Biesinger, L. Lau, A. Gerson, R. Smart, Appl. Surf. Sci. 257 (2010) 887–898.
[27] S. Poulson, P. Parlett, P. Stone, M. Bowker, Surf. Interface Anal. 24 (1996) 811–820.
[28] X. Wang, F. Zhang, B. Xia, X. Zhu, J. Chen, S. Qiu, P. Zhang, J. Li, Solid State Sci. 11 (2009) 655–659.
[29] S. Suárez, J. Martín, M. Yates, P. Avila, J. Blanco, J. Catal. 229 (2005) 227–236.